A FULLY COUPLED FLOW AND GEOMECHANICS MODEL: APPLICATION TO ENHANCED GEOTHERMAL RESERVOIRS

Perapon Fakcharoenphol, Litang Hu, Yu-Shu Wu, Sarinya Charoenwongsa, and Hossein Kazemi

Colorado School of Mines
1500 Illinois street
Golden, CO, 80401
e-mail: pfakchar@mymail.mines.edu

ABSTRACT

This paper presents a fully coupled, fully implicit geomechanics-flow model for fluid and heat in porous media. The model is built and transferred onto the TOUGH2 (Pruess et al, 1999) infrastructure. A staggered grid is used, with flow-related primary variables (pressure, temperature, and phase saturations) located at the center and geomechanics-related variables (displacement components) on the borders of the matrix block.

The model was verified against analytical solutions: (1) 1D heat conduction in deformable media (Jaeger et al., 2007), (2) 1D consolidation (Terzaghi, 1943), and (3) the Mandel and Cryer problem for transversely isotropic poroelastic media (Abousleiman et al., 1996). The model was also verified against the published numerical results of geothermal reservoir modeling (Rutqvist et al., 2008). To demonstrate the capability of the new model, we present a 5-spot well-pattern example of an enhanced geothermal system.

INTRODUCTION

The growing public concern regarding EGS-induced earthquakes causes delays in (and threatens) EGS development worldwide. At least one commercial EGS project (Deep heat mining Basel in Switzerland), has been abandoned because of felt induced earthquakes (Giardini, 2009). Many other commercial EGS fields (Landau in Germany, Berlin in El Salvador) and a conventional geothermal field (The Geysers) have been reported increasing seismic activities once production and injection started (Majer et al.; 2007, Giardini; 2009). As a result, site selection, including earthquake risk assessment, is vital for the development of geothermal fields, especially for a field located in suburb areas.

Production and injection activities alter pressure, temperature, and stress states within geothermal reservoirs, which can cause rock deformation (and even failure) as well as increased seismicity or micro-earthquake (MEQs) events. For example, many studies have demonstrated that MEQs at The Geysers, one of the largest geothermal fields in the world, are associated with water injection and steam extraction (Oppenheimer, 1986; Stark, 2003; Smith et al., 2000; Mossop, 2001; Majer and Peterson, 2005; Majer et al., 2007). Majer et al. (2007) report the correlation between water injection rate and seismic events for a magnitude lower than 1.5—see Fig. 1. Rutqvist et al. (2006, 2007, and 2008) conducted a comprehensive simulation study to simulate production and injection effects on stress changes at The Geysers. Their results indicate that steam extraction could cause seismic activity at shallow depths above the geothermal reservoir, whereas cold-water injection increased seismic activities and could extend the active slip zone several hundred meters below injection zones. These results are consistent with the observed MEQs data.

Majer et al. (2007) point out that large earthquake risks are associated with a large fault system with significant slip. While geological information is required to evaluate the geothermally induced earthquake risks, a coupled flow-geomechanics model can be used to support the analysis of how cold-water injection, steam, or hot-water production could affect the stress field in geothermal reservoirs in a similar manner to that of Rutqvist et al. (2006, 2007, and 2008).

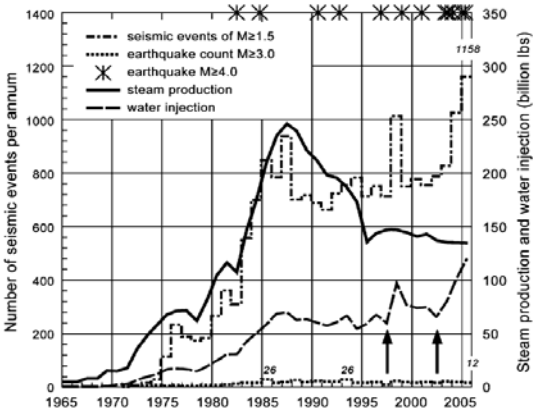

Figure 1. Historical seismicity from 1965 to 2006 at The Geysers: the two arrows indicate the increases in fluid injection in 1997 and 2002 (Majer et al., 2007)

Moreover, change in stress and strain induced by cold-water injection and steam extraction alters hydraulic properties, especially porosity and permeability. Many research efforts (Rutqvist et al., 2002; Davies and Davies, 1999; McKee et al., 1988; Ostensen, 1986) have either experimentally or theoretically investigated the impact of rock deformation on hydraulic properties. As a result, well productivity and injectivity are changed throughout the life of the wells. Thus, to evaluate production from a geothermal field, it is important to include the effect of rock deformation.

In this paper, we present a fully coupled, fully implicit flow-geomechanics model for fluid and heat flow in porous media. Simulated stress and strain can be used to perform shear slip analysis. The developed simulator is built on TOUGH2 (Pruess et al, 1999), a well-established simulator for geo-hydrological-thermal analysis with multiphase, multi-component fluid and heat flow. This simulator is not the first coupled flow-geomechanics model, but it will be among the first fully coupled flow-geomechanics models available in the public domain.

The organization of this paper is as follows. First, we briefly present the mathematical model, similar to TOUGH2. Then, the general concept and numerical treatment of geomechanical formulation are discussed. We compare analytical solutions to numerical results to show the validity of our coupling model. Furthermore, we compare our simulation results of the stress and strain analyses for production-and injection-induced stress changes in The Geysers to Rutqvist et al.'s (2006, 2007, and 2008) simulation results. Finally, we present an application example for 5-spot EGS model.

MATHEMATICAL MODEL

We have developed a fully coupled geomechanics and flow model, based on Charoenwongsa et al. (2010) and Shu (2003). We assume that the boundaries of each simulation grid can move only perpendicularly to its interface as an elastic material, and obeys the generalized Hooke law. Three additional primary variables, namely displacement in x, y, and z direction (u_x, u_y, u_z), are introduced for each grid. Although this numerical scheme is applicable only for a Cartesian grid, it is sufficient to simulate the flow and geomechanical behavior in geothermal reservoirs where geological information (as well as actual subsurface information from drilled wells) is rather sparse and less abundant than that for oil and gas reservoirs.

Reservoir rock is assumed under force equilibrium at all time, and the effect of rock-frame acceleration is ignored. The force equilibrium equations under Newtonian law can be expressed as follows:

$$\nabla \bullet (\Delta\sigma) + \Delta\rho\vec{g} = 0 \tag{1}$$

where $\Delta\sigma$ is the tensor of total stress change from the previous equilibrium condition (here, compression is positive and tension is negative); $\Delta\rho$ is the average bulk-density change from the previous equilibrium condition (typically, this value is very small and dominated by the change in fluid density inside pore space); and $\vec{g}$ is the gravity vector.

In Cartesian coordinates, Eq. (1) can be written as:

$$\begin{bmatrix} \nabla \bullet (\Delta\vec{\sigma}_x) \\ \nabla \bullet (\Delta\vec{\sigma}_y) \\ \nabla \bullet (\Delta\vec{\sigma}_z) + \Delta\rho\vec{g} \end{bmatrix} = \begin{bmatrix} 0 \\ 0 \\ 0 \end{bmatrix} \tag{2}$$

where $\vec{\sigma}_x$ is the stress-component vector acting in the x-direction, composed of normal stress in x-plane (σ_{xx}), shear stress in y-plane (σ_{yx}), and

shear stress in z-plane (σ_{zx}); $\vec{\sigma}_y$ is the stress-component vector acting in the y-direction; and $\vec{\sigma}_z$ is the stress-component vector acting in the z-direction.

Following the numerical framework used in TOUGH2, we can discretize Eq. (2) as follows:

$$\int_{\Gamma_n} \mathbf{F}_j \bullet \mathbf{n} d\Gamma_n + q_j = 0 \tag{3}$$

where $\mathbf{F}_j = \left[\Delta\sigma_{xj} \quad \Delta\sigma_{yj} \quad \Delta\sigma_{zj} + \delta_{zj}\Delta\rho g\right]^T$, $j \in \{x, y, z\}$, and q_j is the external force added to the system.

Stress-Strain Relation

Using the above formulation, we can include different stress-strain relationships. Here, we assume that the rock behaves as a linear poro-thermo-elastic medium with orthotropic material. The stress-strain relationship is given by:

$$\begin{bmatrix} \Delta\sigma_{xx} - \alpha_x\Delta p \\ \Delta\sigma_{yy} - \alpha_y\Delta p \\ \Delta\sigma_{zz} - \alpha_z\Delta p \\ \Delta\sigma_{xy} \\ \Delta\sigma_{yz} \\ \Delta\sigma_{zx} \end{bmatrix} = \begin{bmatrix} \frac{1}{E_x} & -\frac{\nu_{yx}}{E_y} & -\frac{\nu_{zx}}{E_z} & 0 & 0 & 0 \\ -\frac{\nu_{xy}}{E_x} & \frac{1}{E_y} & -\frac{\nu_{zy}}{E_z} & 0 & 0 & 0 \\ -\frac{\nu_{xz}}{E_x} & -\frac{\nu_{yz}}{E_y} & \frac{1}{E_z} & 0 & 0 & 0 \\ 0 & 0 & 0 & 1/G_{xy} & 0 & 0 \\ 0 & 0 & 0 & 0 & 1/G_{yz} & 0 \\ 0 & 0 & 0 & 0 & 0 & 1/G_{zx} \end{bmatrix}^{-1} \begin{bmatrix} \varepsilon_{xx} + \beta_x\Delta T \\ \varepsilon_{yy} + \beta_y\Delta T \\ \varepsilon_{zz} + \beta_z\Delta T \\ 2\varepsilon_{xy} \\ 2\varepsilon_{yz} \\ 2\varepsilon_{zx} \end{bmatrix} \tag{4}$$

where ε_{ij} is normal strain if $i=j$ and shear strain if $i \neq j$, $i, j \in \{x,y,z\}$, E is elastic modulus, ν is passion ratio, G is shear modulus, β is linear thermal expansion, α is Biot coefficient, ΔT is temperature change, and Δp is pressure change.

Also, we assume that the small-strain assumption is adequate for capturing strain in our system. Strain can be calculated from:

$$\varepsilon_{ij} = \frac{1}{2}\left(\frac{\partial u_i}{\partial x_j} + \frac{\partial u_j}{\partial x_i}\right) \qquad i, j \in \{i, j, k\} \tag{5}$$

where, u_x, u_y, and u_z are displacement of the rock frame in x, y, and z-directions, and ε_{ij} is a strain component.

Boundary Treatment

Three types of boundary conditions are discussed here. First, a rigid boundary signifies a stationary rock frame at the reference point. Second, a sliding boundary signifies that the movement of a boundary face occurs exclusively in parallel to the face; no movement in the perpendicular direction to the face is allowed. This type of boundary is commonly used for the outer model boundaries. The last boundary type is a specific stress boundary in which a boundary is subject to a constant stress condition, including normal and shear stresses. Typically, ground surface is modeled by a constant zero-stress boundary. All three boundaries types can be mathematically expressed as follows:

Rigid boundary:

$$u_x = 0, \quad u_y = 0, \quad u_z = 0 \tag{6}$$

Sliding boundary:

$$u_i = 0, \quad \sigma_{ij} = 0 \quad i, j \in \{i, j, k\} \text{ and } i \neq j \tag{7}$$

Specific stress boundary:

$$q_j = \int_s C_{ij} \bullet \vec{n} ds \qquad i, j \in \{i, j, k\} \tag{8}$$

where, C_{ij} is stress component at boundary

Effect of Geomechanics on Mass- and Energy-Balance Equations

Rock deformation affects fluid and heat flow in many ways. The following section explains how we incorporate these effects mathematically.

Permeability and Porosity:

These two quantities, which are among the most important properties for fluid flow, can be significantly affected by rock deformation. Many research efforts (Rutqvist et al., 2002; Davies and Davies, 1999; McKee et al., 1988; Ostensen, 1986) have either experimentally or theoretically investigated the impact of rock deformation on hydraulic properties. A summary of permeability and porosity as functions of stress can be found in Wu et al. (2011). The general mathematical form can be expressed as:

$$k = k(\sigma', \varepsilon) \tag{9}$$

$$\phi = \phi(\sigma', \varepsilon) \tag{10}$$

where k is absolute permeability, ϕ is porosity, σ' is effective stress, and ε is strain.

Mass accumulation:

The total mass within a unit volume of rock may be changed as a result of rock deformation. We account for the mass calculation as:

$$M^{\kappa} = \sum_{\varphi} (1-\varepsilon_v)\phi S_{\varphi}\rho_{\varphi}X_{\varphi}^{\kappa} \tag{11}$$

where, M^{κ} is mass accumulation of component κ, ε_v is volume metric strain, φ is porosity, ρ_{φ} is density of phase φ, S_{φ} is saturation of phase φ, and X_{φ}^{κ} is the mass fraction of component κ in phase φ.

Capillary pressure:

Due to the change in permeability and porosity, Rutqvist et al. (2002) use J-function to correct capillary pressure change.

$$p_c = p_{c,0}\sqrt{\frac{k_0\phi}{k\phi_0}} \tag{12}$$

where, $p_{c,0}$ is nondeformed capillary pressure, k_0, k are initial permeability and deformed permeability, respectively, and φ_0, φ are initial porosity and deformed porosity, respectively,

Fluid mass flow rate:

Not only are intrinsic rock properties altered, but also gridblock surface area is changed due to deformation. Here, we include the effect.

$$q_{\varphi,i} = -F_v\frac{kk_{r\varphi}}{\mu_{\varphi}}\nabla\Phi A_0 \tag{13}$$

where F_v is deformation correction defined as

$$F_{v,i} = \frac{(1-\varepsilon_{jj})(1-\varepsilon_{kk})}{1-\varepsilon_{ii}}$$

and $i,j,k \in \{x,y,z\}$ and $i \neq j \neq k$,

A_0 is initial surface area, k is absolute permeability, $k_{r\varphi}$ is relative permeability of phase φ, and μ is viscosity of phase φ.

MODEL VERIFICATION

Mandel-Cryer Problem for Transversely Isotropic Porous Media

The classical Mandel-Cryer problem involves an infinitely long rectangular specimen, sandwiched at the top and bottom by two rigid frictionless plates; see Fig. 2. The lateral sides are free from normal and shear stresses, as well as pore pressure. At t=0, a force of 2F is applied to the rigid plates. As a result, pore pressure is uniformly increased by the Skempton effect. The pore pressure then dissipates from the side edges.

Abousleiman et al. (1996) extended the classical problem to account for transversely isotropic material. Fig. 2 shows the Mandel-Cryer problem for a transverse isotropic material where (a) case#1 is the axis of material rotational symmetry coinciding with the z-axis, and (b) case#2 is the specimen rotated 90˚.

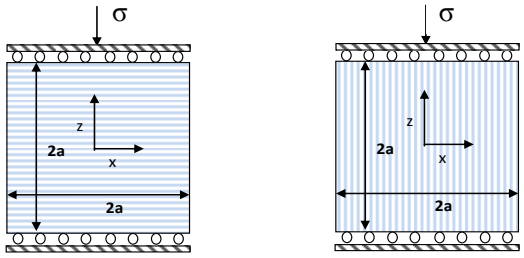

(a) (b)

Figure 2. Problem description (a) Case#1: the axis of material rotational symmetry coincide with z-axis and (b) Case#2: the specimen is rotated by 90˚ from case#1

Table 1. Input parameters for Case#1: Mandel-Cryer problem

Parameters	Value	unit
Young modulus in x and z-direction	20.6, 17.3	GPa
Poisson ratio in xy and xz direction	0.189, 0.246	-
Biot coefficient in x and z-direction	0.733, 0.749	-
Permeability x and z-direction	1.0×10^{-19}, 2.0×10^{-20}	m^2
Porosity	0.1	-
Fluid viscosity	0.001	Pa.s
Pore compressibility	2.0×10^{-10}	1/Pa
Fluid compressibility	4.4×10^{-10}	1/Pa
Applied stress	10	MPa

The simulation results and analytical solution are compared in Fig. 3 and Fig. 4. The figures show good agreement between the two methods, consequently lending credibility to our numerical simulation model.

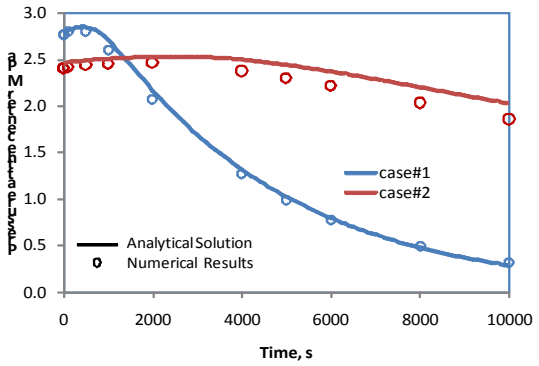

Figure 3. Comparison of pressure solutions between numerical simulation and analytical solution for (1) case#1: material properties according to Table1 and (2) Case#2: the specimen is rotated 90 from Case#1.

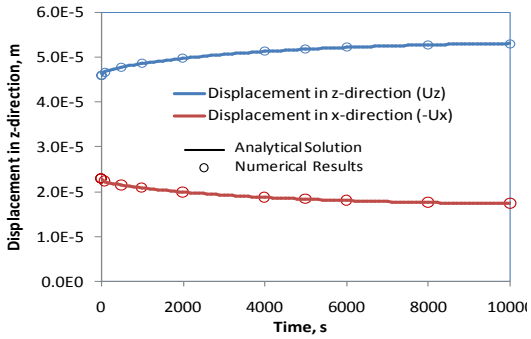

Figure 4. Comparison of displacement in x-direction at the right edge and z-direction at the top of the specimen, between numerical simulation and analytical solution for case#1.

Published Simulation Results: The Geysers Geothermal-Induced Micro-Earthquake Study

In this section, we compare our simulation results (here called 'TOUGH2-EGS') to the published simulation results of The Geysers geothermally induced Micro-Earthquake (MEQs) Study. The study was conducted by Rutqvist et al. (2006, 2007, and 2008), to investigate the effects of steam extraction and water injection in The Geysers.

The Geysers is one of the largest geothermal reservoirs in the world and located in one of the most seismically active regions, Northern California. It is a vapor-dominated geothermal reservoir system, hydraulically confined by low-permeability rock units. Many studies have demonstrated that MEQs at Geysers are associated with water injection and steam extraction (Oppenheimer, 1986; Stark, 2003; Smith et al., 2000; Mossop (2001); Majer and Peterson, 2005; Majer et al., 2007).

Rutqvist et al. (2006, 2007, and 2008) conducted a two-dimensional model simulation representing one-half of a NE-SW cross section of a NW-SE trending of The Geysers geothermal field (Fig. 5). The initial (pre-production) conditions were established through a steady-state multiphase flow simulation. Published data were used to constrain a conceptual Geysers model; detailed model setup can be found in their papers by Rutqvist et al. . (2006, 2007, and 2008). One producer and two injectors are located at the model center (Fig. 6). The steam production and water injection rates over 44 years were scaled to represent the ratio of withdrawal and injection volume to the cross-sectional model.

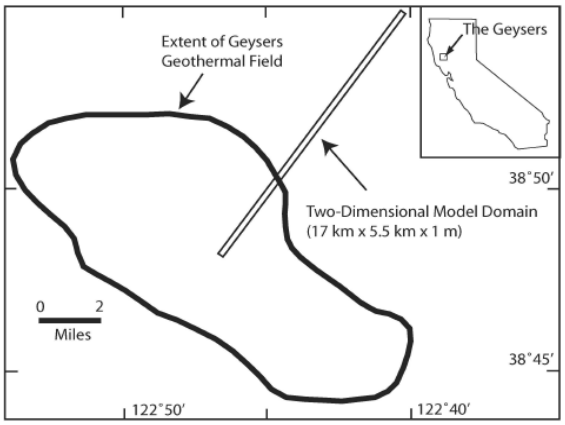

Figure 5. Schematic maps of the study area (Rutqvist and Odenburg, 2008)

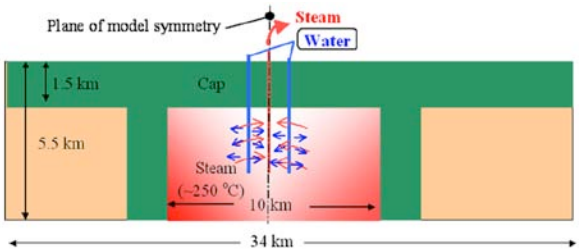

Figure 6. Model schematic: one producer and two injectors (Rutqvist et al. 2008)

The authors employed a coupled flow-geomechanics model using two separated simulators, TOUGH2 (a fluid- and heat-flow simulator) and FLAC (a commercial geomechanics simulator).

TOUGH2 provided pressure and temperature changes to FLAC to calculate stresses changes. Then, stress information from FLAC was returned to TOUGH2 for use in the next time step. This coupling technique is known as "one-way coupling," where pressure and temperature changes influence stresses changes, but stresses changes do not affect the hydraulic properties of current time steps and thus mass- and energy-balance calculations.

The production and injection-rate history of The Geysers was scaled and used to control production and injection rate of the model. This case was set up to investigate both steam-extraction and water-injection effects.

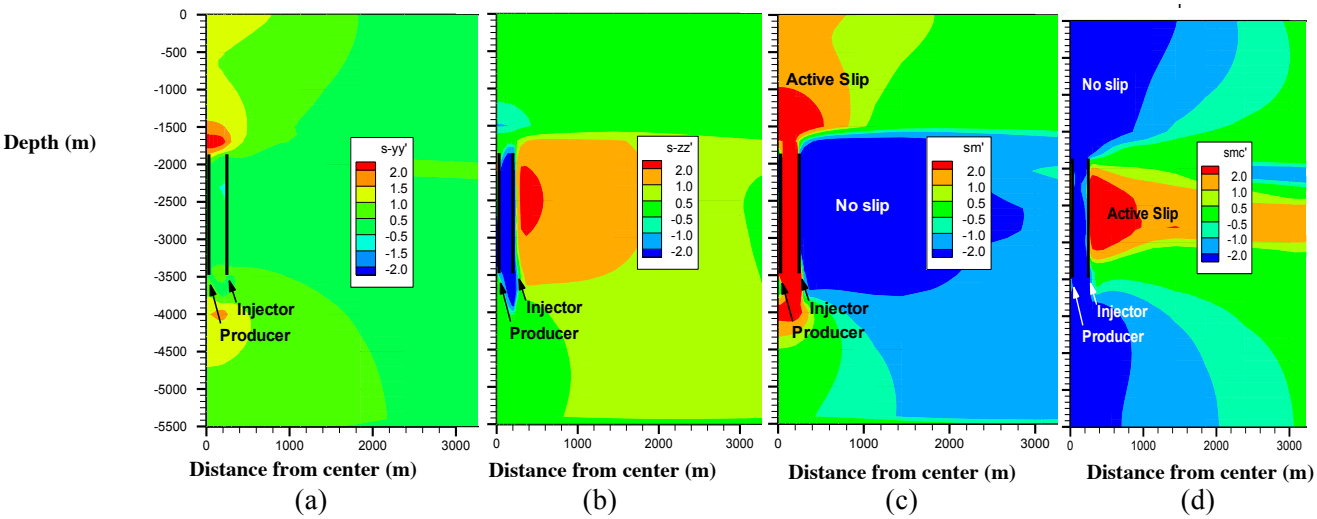

Figure 7. Simulation results using TOUGH2-EGS: (a) change in effective horizontal stress, (b) change in effective vertical stress, (c) $\Delta\sigma'_1$-$\Delta\sigma'_{1c}$ for compressional stress regime ($\sigma'_1 = \sigma'_h$) , where positive value indicates the stress change exceed the critical stress change and can activate MEQs, and (d) $\Delta\sigma'_1$-$\Delta\sigma'_{1c}$ for extensional stress regime ($\sigma'_1 = \sigma'_v$).

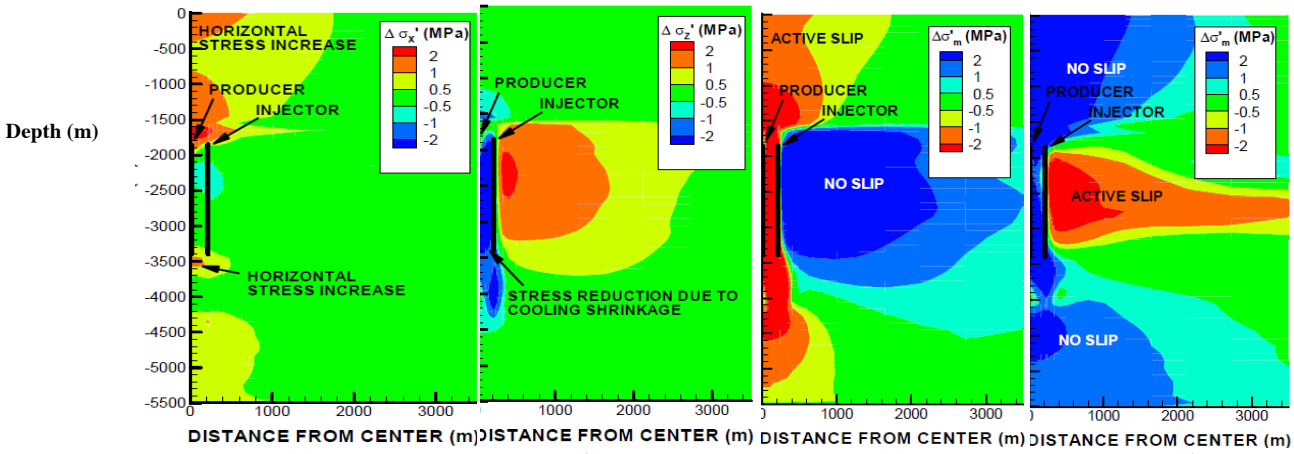

Figure 8. Rutqvist et al. (2007) simulation results: (a) change in effective horizontal stress, (b) change in effective vertical stress, (c) $\Delta\sigma'_1$-$\Delta\sigma'_{1c}$ for compressional stress regime ($\sigma'_1 = \sigma'_h$) , where positive value indicates the stress change exceed the critical stress change and can activate MEQs, and (d) $\Delta\sigma'_1$-$\Delta\sigma'_{1c}$ for extensional stress regime ($\sigma'_1 = \sigma'_v$).

Fig. 7 shows simulation results from TOUGH2-EGS. Fig. 7(a) and Fig. 7(b) depict vertical and horizontal stress changes at the center of the field, respectively. Based on the Mohr-Coulomb

failure criterion, the critical stress change in the maximum principal stress ($\Delta\sigma_{1c}$) is calculated as three times the change in minimum principal stress ($\Delta\sigma_3$) (Rutqvist et al., 2006). Fig. 7(c) and Fig. 7(d) show the indication of active-slip or rock-failure potential, where positive values indicate a failure zone and negative values indicate a stable zone in a compressional stress regime ($\sigma'_1=\sigma'_h$) and an extensional stress regime ($\sigma'_1=\sigma'_v$), respectively. The simulation results indicate that steam extraction yields an active slip regime in shallow depths at the reservoir cap rock for a compressional stress regime, while no slip is expected in the extensional stress regime. These results are consistent with that of published simulation results shown in Fig. 8 (Rutqvist et al., 2006).

APPLICATION EXAMPLE

In geothermal reservoir development, production and injection wells are often drilled in regular geometric patterns. The present problem considers a large well field with wells arranged in a "5-spot" pattern. Because of symmetry, only a quarter of the basic pattern needs to be modeled. Fig. 9 shows a simulation grid in which the grids are refined in the vicinity of injection, while production wells and coarse grids are used elsewhere. The system is initialized as a normal pressure regime where subsurface pressure follows the hydrostatic pressure of the water head, and the temperature gradient is set at 4˚C/km. The reservoir is fully saturated with water. Reservoir rock properties are corresponding to conditions that may typically be encountered in deeper zones of hot and fairly tight geothermal reservoirs.

Continuum Slip Analysis

We employed continuum shear-slip analysis to investigate the extension of potential slip zones, as discussed by Rutqvist et al. (2006). Cold-water injection and steam extraction could cause pressure and temperature changes, as well as alter stress field in reservoirs. To evaluate the potential slip zone, we compared the effective stress to a Mohr-Coulomb failure criterion. In this case, fracture orientations must be known. However, the orientation data may not available. As a precaution, we assumed that preexisting fractures could rotate in any direction. The Mohr-Coulomb failure criterion is given as (Jaeger et al., 2007):

$$\tau_m = S_0 \cos\theta + \sigma_m \sin\theta \qquad (14)$$

where τ_m and σ_m are the two-dimensional maximum shear stress and mean stress in the principal stress plane (σ'_1, σ'_3), defined as:

$$\sigma_m = \frac{1}{2}(\sigma'_1+\sigma'_3),\ \ \tau_m = \frac{1}{2}(\sigma'_1-\sigma'_3) \qquad (15)$$

where S_0 and Θ are the coefficient of internal cohesion and angle of internal friction of the fractures, respectively.

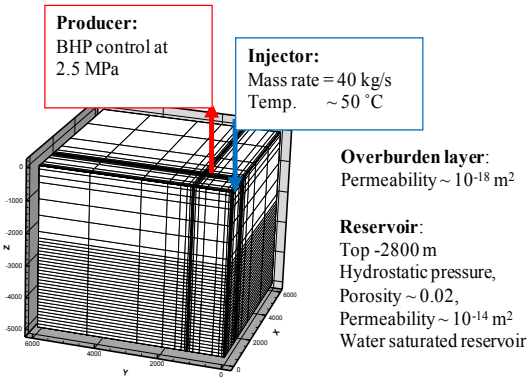

Figure 9. A quarter model for 5-spot pattern

In this example, the potential for shear slip is estimated using zero cohesion ($S_0 = 0$) and a friction angle of 30°, leading to the following criterion for shear slip:

$$\sigma'_1 = 3\sigma'_3 \qquad (16)$$

Thus, shear slip would be induced whenever the maximum principal effective stress exceeds three times the minimum compressive effective stress.

Simulation Results

Fig. 10 and Fig. 11 show simulation results after 6 months of production in the vicinity of the injector and producers, respectively. Around the injector, the temperature is reduced by cooling effects and causes stress reduction, as can be seen from the horizontal stress change following the temperature change pattern—see Fig. 10(a) and (b).

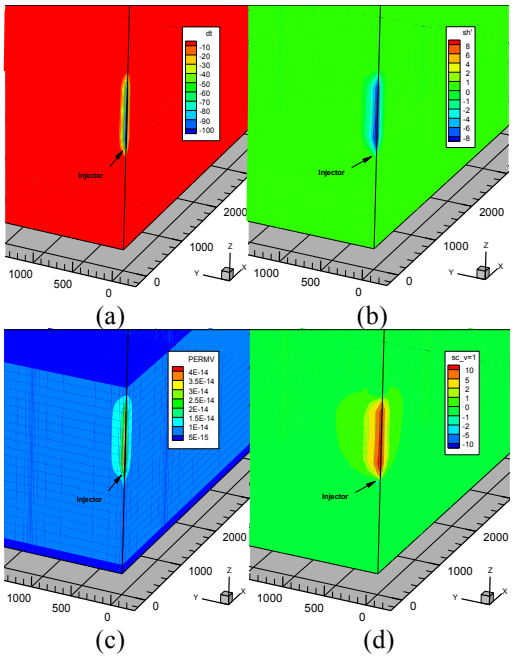

Figure 10. Simulation results at the injector after 6 months: (a) temperature change (b) horizontal stress change, (c) permeability evolution, and, (d) $\Delta\sigma'_v$-$\Delta\sigma_c$ plot for extensional stress regime where positive indicates slip zone.

As a result, permeability is enhanced around the injector, Fig. 11(c). Fig. 11(d) demonstrates active slips zone for the extensional regime (the maximum stress is in the vertical direction). Here, a positive value indicates a failure zone. Clearly, the failure zone evolves around the injector in both cases.

The pressure reduction caused by steam extraction dominates the stress changes around the producer, as the horizontal and vertical stress changes follow the pressure change pattern, Fig. 11 (a) and (b). Consequently, the permeability around the producer declines. Unlike around the injector, Fig. 10 (d) indicates that no active slip zone develops around the producer. As pressure reduction raises the effective normal stress around the producer, the fracture slip potential is reduced. We can see that the active slip zone is developed exclusively around the cold-water injector. Thus, we can study the detailed evolution of the active slip zone around the injector.

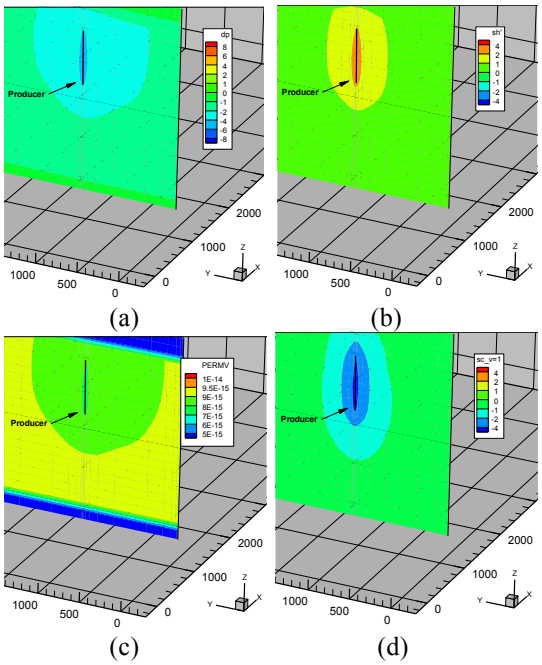

Figure 11. Simulation results at the producer after 6 months: (a) pressure change, (b) vertical stress change, (c) permeability evolution , (d) $\Delta\sigma'_v$-$\Delta\sigma'_c$ plot for extensional stress regime where positive indicates slip zone.

Fig. 12 shows the active-slip-zone evolution around the water injector in both extensional and compressional stress regimes. Under the extensional stress regime, the active slip zone can extend several hundred meters above the injection point during the early production period—Fig. 12(a). Later, the active slip zone extends horizontally only, away from the injector. After five years of production, this zone could extend more than 500 m away from the injector—Fig 12(c). This is because during early production, the pressure drop in the reservoir is insignificant, thus only temperature drop causes stress reduction and dominates the stress field. As temperature change occurs locally, it creates a tension zone in the vertical direction, thus extending the failure zone vertically. However, once the reservoir pressure drop is significant, it raises the effective stress and counteracts the temperature effect. As a result, it diminishes the vertical tension zone and the active slip zone exclusively extends horizontally.

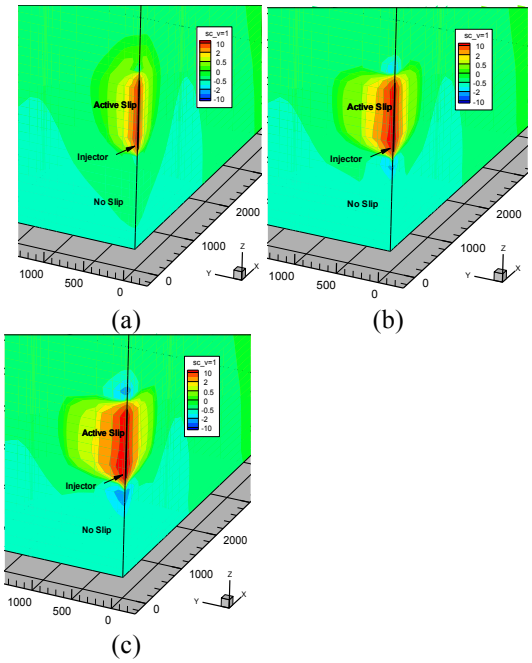

Figure 12. Slip potential plot ($\Delta\sigma'_1$-$\Delta\sigma'_{1c}$) where positive indicates active slip and negative indicates no slip zones for: extensional stress regime (maximum stress is the vertical stress) at (a) 0.5 year, (b) 1.5 year, (c) 5 years.

CONCLUSIONS

In this paper, we describe a fully coupled, fully implicit flow-geomechanics model for fluid and heat flow in porous media. The simulated stress and strain can be used to perform shear slip analysis as well as to analyze the effect of rock deformation on fluid and heat flow in geothermal reservoirs. The developed simulator is built on TOUGH2 (Pruess et al, 1999), a well-established simulator for geo-hydrological-thermal analysis with multiphase, multi-component fluid and heat flow. The developed simulator is not the first coupled flow-geomechanics simulator; however, it will be one of the first fully coupled flow-geomechanics simulators available in the public domain.

We successfully validated our simulator against the analytical solution of Mandel and Cryer problem for transversely isotropic poroelastic media (Abousleiman et al., 1996) and against the published numerical results from a field-application of geothermal reservoir simulation (Rutqvist et al., 2008). In addition, we present an application example for a 5-spot EGS model.

As the public concerns with respect to EGS-induced earthquakes mount, site selection and earthquake risk assessment is vital for EGS development. Our simulator can be used to support the assessment of how cold-water injection and steam or hot-water production could affect the stress field and productivity in geothermal reservoirs—as well as applied to studies of induced seismicity.

ACKOWLEDGMENTS

This work is supported by the U.S. Department of Energy under contract No. DE-EE0002762. Special thanks are due to the Energy Modeling Group (EMG) and Marathon Center of Excellence for reservoir studies (MCERS) at Colorado School of Mines. The authors are also grateful to Jonny Rutqvist at LBNL for the help he provided to this study.

REFERENCES

Aoki, T., C.P. Tan, and W. E. Bamford, Effects of elastic and strength anisotropic on borehole failures in saturated rocks, *Int. J. Rock Mech. Min. Sci.*, **10**, 1031-1034, 1993.

Abousleiman, Y., A. H.-D. Cheng, E. Detournay, L. Cui, and J.-C. Roegiers, Mandel's problem revisited, *Géotechnique,* **46**(2), 187-195, 1996.

Carslaw, H. S., J. C. Jaeger, *Conduction of heat in solids*, second ed. Oxford University Press, USA, 1986.

Charoenwongsa, S., H. Kazemi, J. L. Miskimins, and P. Fakcharoenphol, A fully-coupled geomechanics and flow model for hydraulic fracturing and reservoir engineering applications, *in proceeding of Canadian Unconventional Resources & International Petroleum Conference*, Calgary, Alberta, Canada, 2010.

Davies, J.P., D.K. Davies, Stress-dependent permeability: characterization and modeling, *in proceeding of SPE Annual Technical Conference and Exhibition*, SPE 56813, Houston, Texas, 1999.

Giardini, D, Geothermal Quake Risks Must be Faced, *Nature*, **462**(7275), 848-849, 2009.

Jaeger, J., N.G. Cook, and R. Zimmerman, *Fundamentals of rock mechanics*, forth ed. Wiley-Blackwell, 2007.

Majer, E. L., R. Baria, M. Stark, S. Oates, J. Bommer, B. Smith, and H. Asanuma, Induced Seismicity Associated with Enhanced Geothermal Systems, *Geothermics*, **36**(3), 185-222, 2007.

Majer, E.L., and J.E. Peterson, Application of microearthquake monitoring for evaluating and managing the effects of fluid injection at naturally fractured EGS sites, *Geotherm. Resour. Counc. Trans*, **29**, 103–107, 2005.

McKee, C.R., A.C. Bumb, and R.A. Koenig, Stress-dependent permeability and porosity of coal and other geologic formations, *SPE Formation Evaluation*, **3**(1), 81–91, 1998.

Massachusetts Institute of Technology (MIT), The future of geothermal energy impact of enhanced geothermal systems (EGS) on the United States in the 21st Century, *A report for the U.S. Department of Energy, 2006*.

Mossop, A.P., Seismicity, subsidence and strain at The Geysers geothermal field, *Ph.D. dissertation*, Stanford University, Stanford, CA, 2001.

Ostensen, R.W., The effect of stress-dependent permeability on gas production and well testing, *SPE Formation Evaluation*, **1**(3), pp. 227–235, 1986.

Oppenheimer, D.C., Extensional tectonics at the Geysers geothermal area, California, *J. Geophys. Res.*, **91**, 11463–11476, 1986.

Pruess, K., C. Oldenburg, and G. Moridis, *TOUGH2 user's guide, Version 2.0*, Lawrence Berkeley Laboratory Report LBL-43134, Berkeley, CA, 1999.

Rutqvist, J., J. Birkholzer, F. Cappa,C.M. Odenburg, and C.F. Tsang, Shear-slip analysis in multiphase fluid flow reservoir engineering applications using TOUGH-FLAC, *in proceeding of TOUGH Symposium*, LBNL, Berkeley, California, 2006.

Rutqvist J., and C.M. Odenburg, Technical Report#1: Development of fluid injection strategies for optimizing steam production at The Geysers geothermal field, California, LBNL, Berkeley, California, LBNL-62577, 2007.

Rutqvist, J., and C.M. Odenburg, Analysis of injection-induced micro-earthquakes in a geothermal steam reservoir, The Geysers geothermal field, California, *in proceeding of The 42nd U.S. Rock Mechanics Symposium (USRMS)*, San Francisco, California, 2008.

Rutqvist, J., Y.S. Wu, C.F. Tsang, and G. Bodvarsson, A modeling approach for analysis of coupled multiphase fluid flow, heat transfer, and deformation in fractured porous rock, *Int. J. Rock Mech. Min. Sci.,* **39**, 429–42, 2002.

Smith, J.L.B., J.J. Beall, and M.A. Stark, Induced seismicity in the SE Geysers field, *Geotherm. Resour. Counc. Trans*, **24**, 24–27, 2000.

Stark, M.A, Seismic evidence for a long-lived enhanced geothermal system (EGS) in the Northern Geysers Reservoir, *Geotherm. Resour. Counc. Trans*, **27**, 727-731, 2003.

Shu, T., *Development of Efficient Fully Coupled Geomechanics and Fluid Flow Simulator*, Master Thesis, Stanford University, Stanford, CA, 2003.

Terzaghi, K., *Theoretical Soil Mechanics*, John Wiley and Sons, New York, 1943.

Wu, Y.S., H. Kazemi, T. Xu, K. Zhang, L. Hu, L., X. Zhao, and P. Fakcharoenphol, Quarterly Report 2 of Year 2: Development of Advanced Thermal-Hydrological-Mechanical-Chemical (THMC) Modeling Capabilities for Enhanced Geothermal Systems, *A report for the U.S. Department of Energy, 2011*.